*Article*

# Direct Synthesis of Calcium Lactate through the Reaction of Glycerol with Calcium Hydroxide Catalyzed by Bimetallic AuCu/SiO$_2$ Nanocatalysts

Changqing Li, Xinyue Cui, Aili Wang *, Hengbo Yin *, Yuting Li, Qiao Lin and Junjie Guo

Faculty of Chemistry and Chemical Engineering, Jiangsu University, Zhenjiang 212013, China;
licqup@163.com (C.L.); xycui51@163.com (X.C.)
* Correspondence: alwang@ujs.edu.cn (A.W.); yin@ujs.edu.cn (H.Y.)

**Abstract:** Bimetallic AuCu/SiO$_2$ nanosized catalysts were prepared using the wet chemical reduction technique. From among Au$_{0.1–1.5}$Cu$_{10}$/SiO$_2$ catalysts, the Au$_{0.5}$Cu$_{10}$/SiO$_2$ catalyst gave the highest yield of calcium lactate of 87% at a glycerol conversion of 96% when the reaction of glycerol with calcium hydroxide at a mole ratio of calcium hydroxide to glycerol of 0.8:1 was conducted under an anaerobic atmosphere at 200 °C for 2 h. The interactions between metallic Au$^0$ and Cu$^0$ nanoparticles facilitate calcium lactate formation. The simulation of glycerol consumption rate with an empirical power-function reaction kinetics equation yielded a reaction activation energy of 44.3 kJ·mol$^{-1}$, revealing that the catalytic reaction of glycerol with calcium hydroxide to calcium lactate can be conducted by overcoming a mild energy barrier. The synthesis of calcium lactate through the catalytic reaction of glycerol with calcium hydroxide on a bimetallic AuCu/SiO$_2$ nanosized catalyst under a safe anaerobic atmosphere is an alternative to the conventional calcium lactate production technique through the reaction of expensive lactic acid with calcium hydroxide.

**Keywords:** AuCu/SiO$_2$ catalysts; calcium lactate; glycerol; Ca(OH)$_2$

## 1. Introduction

With the depletion of fossil fuels and the deterioration of the environment by CO$_2$ emissions, the utilization of green and sustainable biomass and its related high value-added fine chemicals has gained much more attention worldwide. Glycerol, a byproduct in biodiesel production, has been produced at a large scale; around 1/10 of total biodiesel production capacity [1]. In addition to this, glycerol is also available in surfactant production from vegetable oils and animal fats. The worldwide glycerol market was estimated at about USD 615 million in 2022 and is expected to reach USD 954 million by 2029 [2]. The high glycerol production capacity makes glycerol conversion to high-value-added chemicals practical and beneficial.

Glycerol molecules of a polyhydroxy nature are multifunctional and can undergo catalytic reactions, such as hydrogenolysis, oxidation, and dehydration, to produce propanediol [3], glyceric acid, glycolic acid [4], dihydroxyacetone [5], glycerol carbonate [6], lactic acid [7–9], and calcium lactate [10]. From among them, calcium lactate can be used as a calcium supplement, antimicrobial agent, and in a variety of food additives in food, medicine, and feed fields.

Calcium lactate is commercially produced through the neutralization reaction of lactic acid with calcium hydroxide. For the raw material lactic acid, numerous studies have disclosed that noble metal catalysts, such as Au [11,12], Pt [13], and AuPt [14], can catalyze glycerol oxidation with gaseous O$_2$ to lactic acid at reaction temperatures in a range of 60–100 °C, yielding lactic acid selectivities of 16%, 92.3%, 69.3%, and 83% at glycerol conversions of 15%, 82.4%, 100%, and 100%. Although noble metal catalysts can catalyze glycerol oxidation to lactic acid at mild reaction temperatures of around 95 °C, lower lactic

acid selectivity at higher glycerol conversion rates and a higher noble metal catalyst cost limit their practical applications in lactic acid production.

Researchers have recently reported that non-precious metals exhibit impressively catalytic activities in hydrothermal glycerol conversion to lactic acid in alkaline aqueous solutions under an anaerobic atmosphere. It was reported that the glycerol conversion and lactic acid selectivity on the Cu/ZIF-8 catalyst were 97.5% and 84.2% when the glycerol conversion was conducted in sodium hydroxide aqueous solutions under an anaerobic $N_2$ atmosphere at 230 °C for 8 h [15]. When the synthesis of lactic acid through hydrothermal glycerol conversion in sodium hydroxide aqueous solutions was conducted on a 20CuHT catalyst bed at 240 °C, the glycerol conversion and lactic acid yield were around 96.5% and 64%, respectively [16]. It was also reported that when the hydrothermal conversion of glycerol to lactate was conducted in calcium hydroxide aqueous solutions at 230 °C, the lactate selectivity was above 91% at a glycerol conversion of around 93% [10].

Cobalt-derived catalysts were also utilized in the conversion of glycerol to lactic acid in sodium hydroxide aqueous solutions at a higher reaction temperature of 250 °C [17]. At the comparable glycerol conversion of around 53.5%, the selectivities of lactic acid reached 90% for $Co_3O_4/CeO_2$, 78% for $Co_3O_4/ZrO_2$, and 68% for $Co_3O_4/TiO_2$. Furthermore, Ye et al. [18,19] found that CaO and CaO/CuO catalysts could effectively catalyze the conversion of glycerol to lactic acid with a yield of 40.8% at a glycerol conversion of 97.8% and after esterification with methanol, the methyl lactate yield reached 57% at a glycerol conversion of 94%.

Active components and surface acidic/basic performance play important roles in catalytic glycerol conversion to lactic acid [10,15–17]. Considering that noble metal catalysts can catalyze glycerol conversion at a mild reaction temperature, whereas copper-based catalysts exhibit higher lactic acid selectivity at a higher temperature, we suggest that combining non-precious Cu with noble Au could produce good catalytic performance in glycerol conversion to lactate in an alkaline aqueous solution under anaerobic atmosphere.

In our present work, $SiO_2$-nanoparticle-supported bimetallic AuCu nanocatalysts were prepared using a wet chemical reduction technique. The catalytic activity of the bimetallic $AuCu/SiO_2$ nanocatalyst in the synthesis of calcium lactate through the reaction of glycerol with calcium hydroxide under an anaerobic atmosphere was assessed. And a power-function type reaction kinetics equation for glycerol consumption rate was simulated to assess the impacts of reaction parameters. Our present work reveals that calcium lactate can be effectively synthesized through the direct reaction between biomass glycerol and $Ca(OH)_2$ catalyzed by the bimetallic $AuCu/SiO_2$ catalyst, which is a sustainable methodology for the synthesis of calcium lactate instead of the conventional production technique through the reaction of expensive lactic acid with calcium hydroxide.
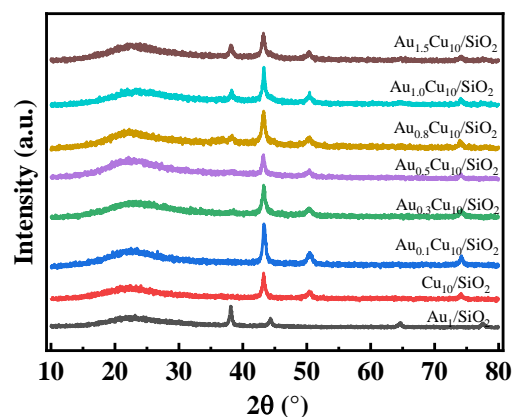
## 2. Results and Discussion

### 2.1. XRD Analysis

The X-ray diffractograms of $Au_1/SiO_2$, $Cu_{10}/SiO_2$, and $Au_{0.1–1.5}Cu_{10}/SiO_2$ catalysts are illustrated in Figure 1. For all catalysts, wide XRD peaks centering at $2\theta = 22.3°$ are ascribed to that of amorphous $SiO_2$ nanoparticle support.

The XRD peaks of the $Cu_{10}/SiO_2$ catalyst centered at $2\theta = 43.3, 50.5,$ and $74.3°$ are assigned to the (1 1 1), (2 0 0), and (2 2 0) crystal planes of metallic $Cu^0$ (JCPDS 04-0836), respectively. For $Au_{0.1–1.5}Cu_{10}/SiO_2$ catalysts, their XRD peaks at $2\theta = 43.3, 50.5,$ and $74.2°$ are also assigned to the (1 1 1), (2 0 0), and (2 2 0) crystal planes of metallic $Cu^0$ (JCPDS 04-0836). Calculated with the utilization of the Scherrer equation, crystallite sizes of metallic Cu (1 1 1) in the $Au_{0.1–1.5}Cu_{10}/SiO_2$ catalysts decreased from 18.4 to 12.1 nm with the increase in Au content from 0% to 1.5 wt%. The presence of the Au component inhibited the crystal growth of the $Cu^0$ component.

The XRD peaks of the $Au_{1.0}/SiO_2$ catalyst centered at $2\theta = 38.1, 44.4, 64.6,$ and $77.5°$ are ascribed to (1 1 1), (2 0 0), (2 2 0), and (3 1 1) crystal planes of face-centered cubic $Au^0$ (JCPDS 99-0056), respectively. For the $Au_{0.1–1.5}Cu_{10}/SiO_2$ catalysts, at lower Au contents

of less than 0.8 wt%, there were no XRD peaks for metallic $Au^0$ detected, whereas with larger Au contents of 0.8 wt%, 1.0 wt%, and 1.5 wt%, only XRD peaks ascribed to the (1 1 1) crystal plane of metallic $Au^0$ were detected, and XRD peaks centered at 38.3, 38.2, and 38.2°, respectively. As compared to the $Au_{1.0}/SiO_2$ catalyst, the positive shift in XRD peaks (1 1 1) of $AuCu/SiO_2$ catalysts should be caused by interactions between Cu and Au components.



**Figure 1.** XRD patterns of the $Au_1/SiO_2$, $Cu_{10}/SiO_2$, and bimetallic $AuCu/SiO_2$ catalysts.

According to the Scherrer equation, the crystallite sizes of Au (1 1 1) of $Au_{0.8}Cu_{10}/SiO_2$, $Au_{1.0}Cu_{10}/SiO_2$, $Au_{1.5}Cu_{10}/SiO_2$, and $Au_{1.0}/SiO_2$ catalysts were 6.7, 9.9, 12.2, and 18.1 nm, respectively. The results reveal that Au components in catalysts are at a nanosized scale. For the same Au content, the crystallite size of the Au component in the $Au_{1.0}Cu_{10}/SiO_2$ catalyst is obviously less than that in the $Au_{1.0}/SiO_2$ catalyst, which could be interpreted as the interactions between Cu and Au components inhibiting the crystal growth of the metallic $Au^0$ nanoparticles.

### 2.2. TEM and HRTEM Analyses

TEM images show that particle sizes of $SiO_2$ support are in a range of 9–24 nm and center at 13 nm (Figure 2a–d). Average particle sizes and particle size distributions of metallic $Cu^0$ and $Au^0$ nanoparticles of the $Cu_{10}/SiO_2$ and $Au_1/SiO_2$ catalysts are 8.2, 5.3–12.3 and 3.4, 1.6–6.6 nm, respectively (Figure 2a,b). Average particle sizes and particle size distributions of metallic $Cu^0$ and $Au^0$ nanoparticles of the $Au_{0.1}Cu_{10}/SiO_2$ and $Au_{0.5}Cu_{10}/SiO_2$ are 8.2, 5.4–11.4; 2.9, 1.4–4.6 and 7.5, 5.1–10.7; and 2.8, 1.1–4.7 nm (Figure 2c,d). TEM and HRTEM images clearly disclose that Cu and Au components are present at a nanosized scale in catalysts.

The lattice fringes of $Au_1/SiO_2$ and $Au_{0.1}Cu_{10}/SiO_2$ catalysts show that gold and copper components are present in metallic states (Figure 2e,f). The small-sized metallic Cu and Au nanoparticles were anchored and dispersed on the surfaces of $SiO_2$ nanoparticles. The adjacent Cu and Au nanoparticles may have interactions.
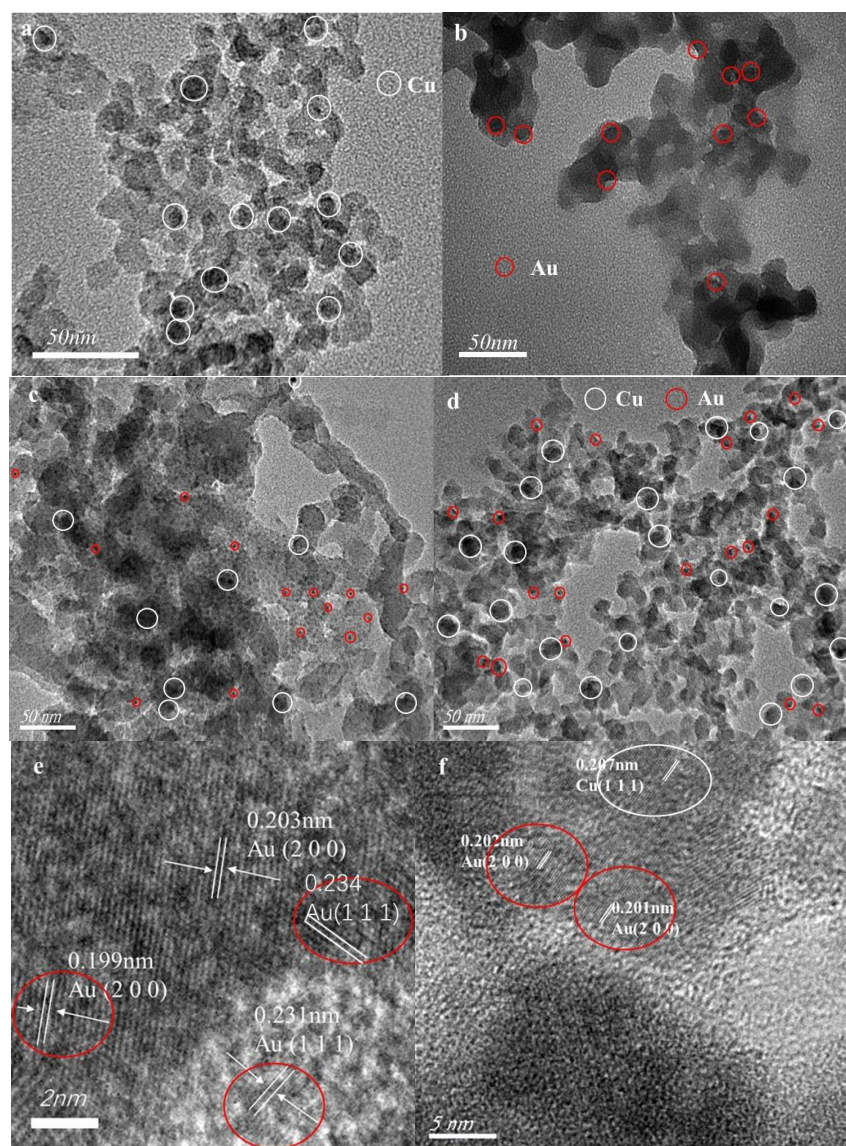
### 2.3. XPS Analysis

Figure 3a shows that the binding energies of Si2p of $SiO_2$ support, $Au_{1.0}/SiO_2$, $Cu_{10}/SiO_2$, $Au_{0.1}Cu_{10}/SiO_2$, and $Au_{0.5}Cu_{10}/SiO_2$ catalysts decrease from 103.7 to 103.2 eV with the introduction of Cu and Au components. The obvious shift of Si2p with the introduction of Cu and Au components reveals that there are interactions between $SiO_2$ support and metallic $Cu^0$ and $Au^0$ components. Considering that the electronegativity of $Si^{4+}$ (>14.15) is much larger than that of Au atoms (2.54) and Cu atoms (1.9) [20,21], the negative shift in Si2p indicates that electrons of Au and Cu components probably transfer to silicon ($Si^{4+}$) components.

For the $Cu_{10}/SiO_2$, $Au_{0.1}Cu_{10}/SiO_2$, and $Au_{0.5}Cu_{10}/SiO_2$ catalysts, there were no characteristic satellite Cu2p peaks around 944 eV for $Cu^{2+}$ observed (Figure 3b), which indicates that copper components in the above-mentioned catalysts are present at metallic
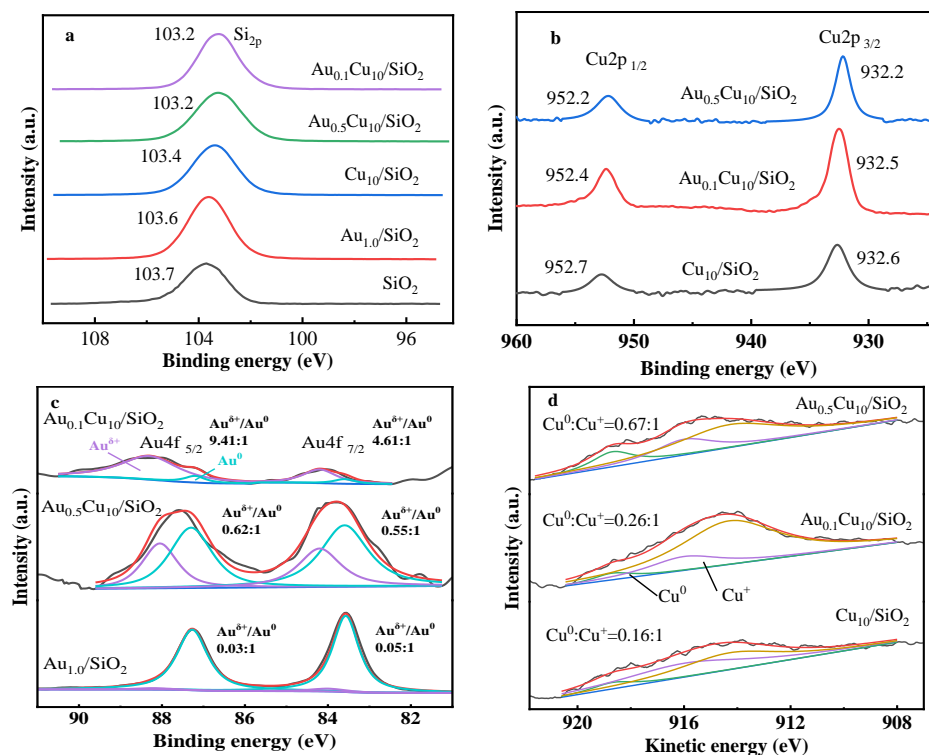
$Cu^0$ and/or $Cu^+$ states [22]. Binding energies of $Cu2p_{1/2}$ and $Cu2p_{3/2}$ of the $Cu_{10}/SiO_2$, $Au_{0.1}Cu_{10}/SiO_2$, and $Au_{0.5}Cu_{10}/SiO_2$ catalysts were 952.7, 932.6; 952.4, 932.5; 952.2, and 932.2 eV. The addition of the Au component makes the Cu2p peaks shift negatively.



**Figure 2.** TEM images of the (**a**) $Cu_{10}/SiO_2$, (**b**) $Au_1/SiO_2$, (**c**) $Au_{0.1}Cu_{10}/SiO_2$, and (**d**) $Au_{0.5}Cu_{10}/SiO_2$ catalysts and HRTEM images of (**e**) $Au_1/SiO_2$ and (**f**) $Au_{0.1}Cu_{10}/SiO_2$ catalysts.

Binding energies of $Au4f_{5/2}$ and $Au4f_{7/2}$ of the $Au_{1.0}/SiO_2$, $Au_{0.1}Cu_{10}/SiO_2$, and $Au_{0.5}Cu_{10}/SiO_2$ catalysts were 87.2, 83.6; 88.2, 84.1; and 87.6, 83.8 eV (Figure 3c). The presence of metallic $Cu^0$ in catalysts makes the Au4f shift positively. To reveal surface chemical valences of $Au^0$ nanoparticles in $Au_{1.0}/SiO_2$, $Au_{0.1}Cu_{10}/SiO_2$, and $Au_{0.5}Cu_{10}/SiO_2$ catalysts, their XPS peaks were deconvoluted by utilizing the Gaussian–Lorentzian bands with peak positions at ca.87.2 and 83.6 eV for $Au4f_{5/2}$ and $Au4f_{7/2}$ of $Au^0$ and ca. 88.2 and 84.2 eV for $Au4f_{5/2}$ and $Au4f_{7/2}$ of $Au^{\delta+}$ [23,24]. The deconvoluting results show that the area ratios of $Au^{\delta+}/Au^0$ for $Au4f_{5/2}$ and $Au4f_{7/2}$ of $Au_{1.0}/SiO_2$, $Au_{0.1}Cu_{10}/SiO_2$, and $Au_{0.5}Cu_{10}/SiO_2$ catalysts were 0.03:1, 0.05:1; 9.41:1, 4.61:1; and 0.62:1, 0.55:1, respectively. The shifts in Au and Cu peaks reveal that there are interactions between $Au^0$ and $Cu^0$ nanoparticles in $AuCu/SiO_2$ catalysts through the electron transfer from the Au component to the Cu component, which is consistent with that observed by XRD analysis. Interestingly, it was found that the shift extent of the Au4f of $Au_{0.1}Cu_{10}/SiO_2$ was larger than that of

$Au_{0.5}Cu_{10}/SiO_2$. It could be explained because with a relatively lower Au content, $Au^0$ nanoparticles could efficiently interact with $Cu^0$ nanoparticles, whereas with a higher Au content, some of the $Au^0$ nanoparticles are probably apart from the surfaces of the $Cu^0$ nanoparticles.
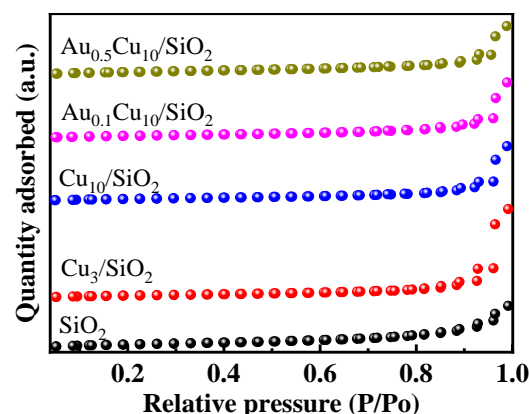


**Figure 3.** XPS of (**a**) Si2p, (**b**) Cu2p, and (**c**) Au4f of the $SiO_2$ support, $Au_{1.0}/SiO_2$, $Cu_{10}/SiO_2$, $Au_{0.1}Cu_{10}/SiO_2$, and $Au_{0.5}Cu_{10}/SiO_2$ catalysts and (**d**) Cu XAES of the $Cu_{10}/SiO_2$, $Au_{0.1}Cu_{10}/SiO_2$, and $Au_{0.5}Cu_{10}/SiO_2$ catalysts.

To reveal the surface chemical valences of $Cu^0$ nanoparticles in $Cu_{10}/SiO_2$, $Au_{0.1}Cu_{10}/SiO_2$, and $Au_{0.5}Cu_{10}/SiO_2$ catalysts, their XAES peaks were deconvoluted by utilizing the Gaussian–Lorentzian bands with peak positions at 916 eV for $Cu^+$ and 918.7 eV for metallic $Cu^0$, and 914.3 eV for other orbital electrons [25]. The deconvoluting results show that the area ratios of $Cu^0/Cu^+$ of $Cu_{10}/SiO_2$, $Au_{0.1}Cu_{10}/SiO_2$, and $Au_{0.5}Cu_{10}/SiO_2$ catalysts were 0.16:1, 0.26:1, and 0.67:1, respectively (Figure 3d). The electronegativities of $Cu^{2+}$, $Cu^+$, and $Au^0$ were 10.28, 5.04, and 2.54, respectively [20,21]. The results disclose that the $Au^0$ nanoparticles present in $AuCu/SiO_2$ catalysts could transfer electrons to $Cu^{2+}$ and even $Cu^+$ components, which prevents the oxidation of $Cu^0$ nanoparticles to some extent.

On the other hand, the atomic ratios of Au/Cu in $Au_{0.1}Cu_{10}/SiO_2$ and $Au_{0.5}Cu_{10}/SiO_2$ catalysts were 0.32:100 and 1.61:100, respectively. The XPS analysis showed that the atomic ratios of Au/Cu for $Au_{0.1}Cu_{10}/SiO_2$ and $Au_{0.5}Cu_{10}/SiO_2$ catalysts were 0.36:100 and 8.64:100. These results disclose that the surface compositions of the Au component are larger than the bulk ones. It is reasonable to suggest that metallic $Au^0$ nanoparticles could anchor at surfaces of metallic $Cu^0$ nanoparticles.

### 2.4. $N_2$ Physisorption

As illustrated in Figure 4, nitrogen adsorption/desorption curves of representative samples show that the $N_2$ adsorption/desorption isotherms belong to the III type. The $SiO_2$ nanoparticle support has a large surface area of up to 221.2 $m^2 \cdot g^{-1}$ (Table 1). For the $Cu_{3-10}/SiO_2$ catalysts, their surface areas decreased from 151.3 to 132.4 $m^2 \cdot g^{-1}$ with the increase in Cu content from 3 wt% to 10 wt%. Their pore volumes and pore sizes were larger than those of the $SiO_2$ support, respectively.

**Figure 4.** Nitrogen adsorption/desorption curves of the $SiO_2$ support and representative $Cu/SiO_2$ and $AuCu/SiO_2$ catalysts.

**Table 1.** Structural properties of the $SiO_2$, $Cu/SiO_2$, $Au/SiO_2$, and $AuCu/SiO_2$ catalysts.

| Catalysts | $S_{BET}$ (m$^2$·g$^{-1}$) | $V_{pore}$ (cm$^3$·g$^{-1}$) | $D_{pore}$ (nm) |
|---|---|---|---|
| $SiO_2$ | 221.4 | 0.57 | 11.10 |
| $Cu_3/SiO_2$ | 151.3 | 1.14 | 28.34 |
| $Cu_5/SiO_2$ | 141.0 | 1.07 | 26.67 |
| $Cu_{10}/SiO_2$ | 132.4 | 0.71 | 21.06 |
| $Au_1/SiO_2$ | 104.2 | 0.75 | 28.16 |
| $Au_{0.1}Cu_{10}/SiO_2$ | 151.9 | 0.73 | 18.83 |
| $Au_{0.3}Cu_{10}/SiO_2$ | 212.2 | 0.73 | 15.05 |
| $Au_{0.5}Cu_{10}/SiO_2$ | 177.8 | 0.65 | 14.07 |
| $Au_{0.8}Cu_{10}/SiO_2$ | 160.5 | 0.60 | 12.76 |
| $Au_{1.0}Cu_{10}/SiO_2$ | 105.0 | 0.62 | 11.96 |
| $Au_{1.5}Cu_{10}/SiO_2$ | 104.6 | 0.60 | 11.91 |

When the second metal, Au, was introduced, the surface areas of the $Au_{0.1-1.5}Cu_{10}/SiO_2$ catalysts increased to 212.2 m$^2$·g$^{-1}$ with the increase in Au content to 0.3 wt% and then decreased to 104.6 m$^2$·g$^{-1}$ with the further increase in the Au content to 1.5 wt%. Both pore volume and pore size decreased with the increase in Au content in $Au_{0.1-1.5}Cu_{10}/SiO_2$ catalysts. The small-sized Au nanoparticles easily choked catalyst pores, which lead to a decrease in the specific surface area of the $Au_1/SiO_2$ catalyst. When Cu nanoparticles were present in bimetallic $CuAu/SiO_2$ catalysts, large-sized Cu nanoparticles reduced the choking to some extent, causing an increase in the surface area. However, the choking effect by Au nanoparticles increased with a higher content of Au nanoparticles, which decreased the specific surface area of the catalyst.

The $Cu_{3-10}/SiO_2$, $Au_1/SiO_2$, and $Au_{0.1-1.5}Cu_{10}/SiO_2$ catalysts have large surface areas and pore sizes, which could supply a large amount of catalytic active sites and diminish mass transfer resistance in pores.

### 2.5. Catalytically Hydrothermal Conversion of Glycerol with Calcium Hydroxide to Calcium Lactate

#### 2.5.1. Impact of Catalyst Composition

When the reaction of glycerol with calcium hydroxide at an initial mole ratio of calcium hydroxide to glycerol of 0.8:1 was catalyzed on $Cu_{3-10}/SiO_2$, $Au_1/SiO_2$, and $Au_{0.1-1.5}Cu_{10}/SiO_2$ catalysts in aqueous solutions at 200 °C for 2 h, for the $Cu_{3-10}/SiO_2$ catalysts, the glycerol conversion, calcium lactate yield, and carbon balance increased with the increase in Cu content. From among $Cu_{3-10}/SiO_2$ catalysts, the $Cu_{10}/SiO_2$ catalyst gave the maximum glycerol conversion of 67% and a calcium lactate yield of 58% (Table 2). Larger metallic Cu content facilitates calcium lactate formation and inhibits byproduct formation.

**Table 2.** Catalytic performance of the $SiO_2$, $Cu/SiO_2$, $Au/SiO_2$, and $AuCu/SiO_2$ catalysts.

| Catalysts | Glycerol Conversion (%) | Product Selectivity (%) | | | | Yield (%) | Carbon Balance (%) |
|---|---|---|---|---|---|---|---|
| | | OA | FA | LA | AA | LA | |
| $Cu_3/SiO_2$ | 22 | 0.2 | 5 | 60 | 8 | 13 | 73.2 |
| $Cu_5/SiO_2$ | 44 | 0.1 | 1 | 77 | 2 | 34 | 80.1 |
| $Cu_{10}/SiO_2$ | 67 | 0.2 | 2 | 87 | 1 | 58 | 90.2 |
| $Au_1/SiO_2$ | 24 | 0.3 | 0.2 | 4 | 1 | 1 | 5.5 |
| $Au_{0.1}Cu_{10}/SiO_2$ | 81 | 0.2 | 2 | 94 | 3 | 76 | 99.2 |
| $Au_{0.3}Cu_{10}/SiO_2$ | 90 | 0.2 | 2 | 93 | 3 | 84 | 98.2 |
| $Au_{0.5}Cu_{10}/SiO_2$ | 96 | 0.2 | 2 | 91 | 3 | 87 | 96.2 |
| $Au_{0.8}Cu_{10}/SiO_2$ | 97 | 0.2 | 2 | 89 | 4 | 86 | 95.2 |
| $Au_{1.0}Cu_{10}/SiO_2$ | 99 | 0.2 | 1 | 87 | 3 | 86 | 91.2 |
| $Au_{1.5}Cu_{10}/SiO_2$ | 100 | 0.2 | 2 | 84 | 4 | 84 | 90.2 |

Glycerol aqueous solution, 2.0 mol·$L^{-1}$; initial mole ratio of calcium hydroxide to glycerol at 0.8:1; catalyst, 9.2 g·$L^{-1}$; reaction time, 2.0 h; reaction temperature, 200 °C. OA, oxalate; FA, formate; LA, lactate; AA, acetate.

The monometallic $Au_1/SiO_2$ catalyst exhibits poor catalytic performance in the reaction of glycerol with calcium hydroxide to calcium lactate, which leads to a much lower carbon balance value of 6%. This phenomenon is worthy of further investigation when metallic Au is solely used as the active component.

When metallic $Au^0$ was introduced into the $Cu_{10}/SiO_2$ catalyst, glycerol conversions increased with the increase in Au content in bimetallic $Au_{0.1-1.5}Cu_{10}/SiO_2$ catalysts. When Au contents were 1 wt% and 1.5 wt%, the glycerol conversions were above 99%. At a Au content of 0.5–1.0 wt%, the calcium lactate yields were above 86% with glycerol conversions ranging from 96% to 99%. As compared to the catalytic activity of the $Cu_{3-10}/SiO_2$ catalysts, the bimetallic $AuCu/SiO_2$ catalyst exhibited high catalytic performance for calcium lactate synthesis through the hydrothermal reaction, starting from glycerol and calcium hydroxide at the reaction temperature of 200 °C.
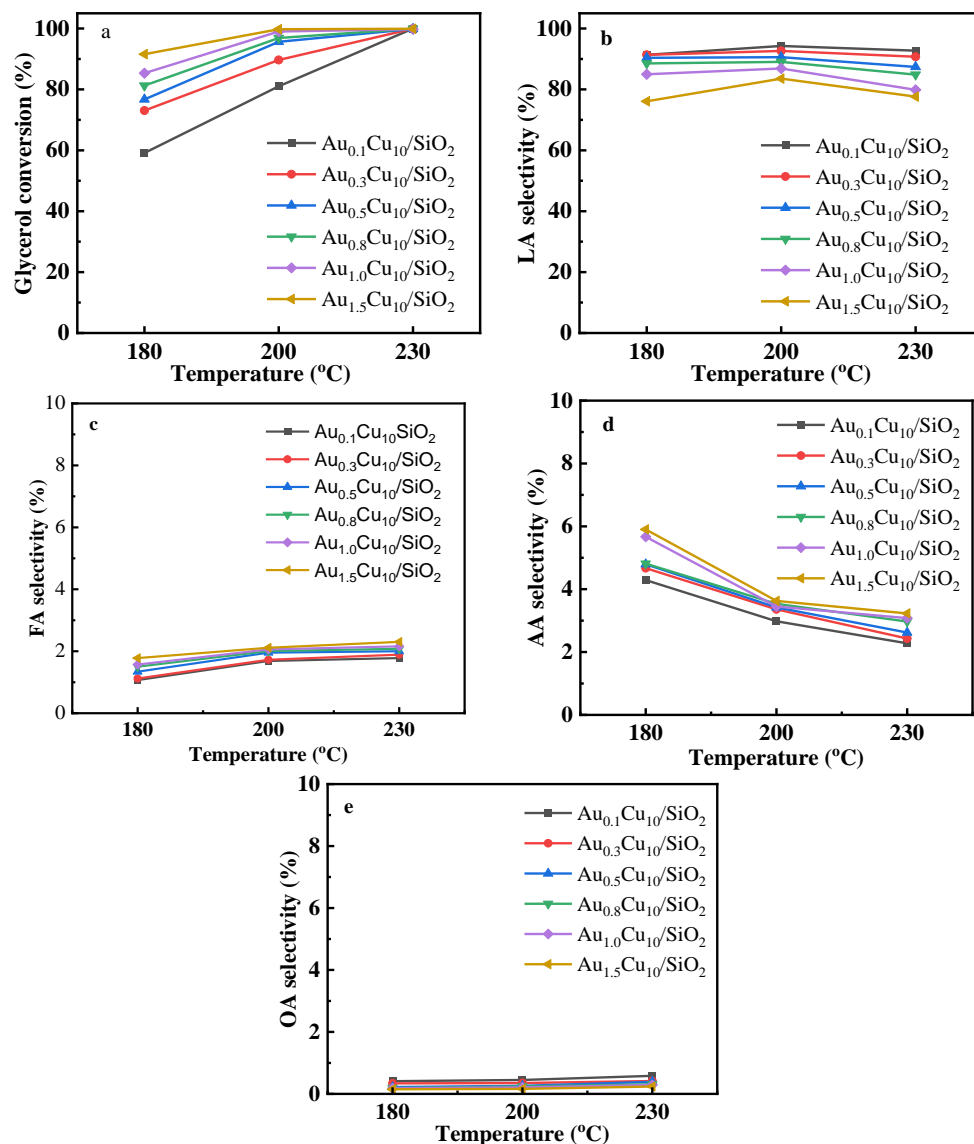
It has been reported that small-sized CuO particles facilitate the conversion of glycerol to lactic acid [26]. However, when Cu-ZnO@C catalysts with metallic Cu particle sizes of 36.9, 67.8, and 93.6 nm catalyzed glycerol conversion to lactic acid, the Cu-ZnO@C catalyst with a metallic Cu particle size of 67.8 nm gave the highest lactic acid yield [27]. As compared to the Cu(16)/$ZrO_2$ catalyst with a metallic Cu crystallite size of 44.5 nm, the Cu(16)HAP catalyst with a metallic Cu crystallite size of 33.8 nm exhibited a high glycerol conversion of 99% and a high lactic acid selectivity of 87% after reacting at 230 °C for 8 h [28]. Liu et al. [29] reported that the metallic Cu nanoparticle with a mean particle size of 11 nm exhibited the highest catalytic activity when $Cu/SiO_2$ catalysts with mean metallic Cu particle sizes of 4–38 nm catalyzed xylitol hydrogenolysis. Generally, both the metallic Cu particle size and support type co-affect catalytic reactions.

In our present research, although the $Cu_{10}/SiO_2$, $Au_{0.1}Cu_{10}/SiO_2$, and $Au_{0.5}Cu_{10}/SiO_2$ catalysts had comparable metallic Cu nanoparticle sizes (around 8.0 nm), glycerol conversions on the $Au_{0.1}Cu_{10}/SiO_2$ and $Au_{0.5}Cu_{10}/SiO_2$ catalysts were 1.21 and 1.43 times those on the $Cu_{10}/SiO_2$ catalyst. The result clearly indicates that the interaction between $Au^0$ and $Cu^0$ nanoparticles improves the catalytic activity.

### 2.5.2. Impact of Reaction Temperature

Catalytic activities of the $Au_{0.1-1.5}Cu_{10}/SiO_2$ catalysts in the reaction of glycerol with calcium hydroxide at an initial mole ratio of calcium hydroxide to glycerol of 0.8:1 to calcium lactate were investigated at 180, 200, and 230 °C for 2 h (Figure 5). When the Au content in $AuCu/SiO_2$ catalysts was above 0.3 wt%, the glycerol conversion was more than 95% at the temperature of 200 °C. As the temperature was raised to 230 °C, on all the $Au_{0.1-1.5}Cu_{10}/SiO_2$ catalysts, glycerol was almost completely converted (Figure 5a).

**Figure 5.** Reaction of glycerol with calcium hydroxide catalyzed by the $Au_{0.1-1.5}Cu_{10}/SiO_2$ catalysts. Glycerol aqueous solution, 2 mol·$L^{-1}$; initial mole ratio of calcium hydroxide to glycerol at 0.8:1; catalyst, 9.2 g·$L^{-1}$; reaction time, 2 h. (**a**) Glycerol conversion and (**b–e**) selectivities of calcium lactate, formate, acetate, and oxalate.

When bimetallic $AuCu/SiO_2$ catalysts with Au content of 0.1–0.5 wt% catalyzed the reaction at 180 and 200 °C, the calcium lactate selectivity was above 90% (Figure 5b). When bimetallic $AuCu/SiO_2$ catalysts with Au content of 0.8–1.5 wt% catalyzed the reaction at 180–230 °C, the calcium lactate selectivity was lower than 90%. The $Au_{0.5}Cu_{10}/SiO_2$ catalyst gave the highest calcium yield at the reaction temperature of 200 °C.

At the reaction temperatures of 180–230 °C on the $Au_{0.1-1.5}Cu_{10}/SiO_2$ catalysts, the selectivities of formate, acetate, and oxalate were below 2%, 6%, and 1%, respectively (Figure 5c–e). The $Au_mCu_{10}/SiO_2$ catalysts with a larger Au content gave slightly higher byproduct selectivity than those with a smaller Au content.

The catalysis results show that at a Au content of 0.5 wt%, the $Au_{0.5}Cu_{10}/SiO_2$ catalyst is more profitable for calcium lactate formation through the catalytic reaction of glycerol with calcium hydroxide. As certified by the XPS analysis, at a Au content of 0.5 wt% or less, Au nanoparticles could efficiently interact with Cu nanoparticles, which improves the reaction of glycerol with calcium hydroxide to calcium lactate. At a larger Au content, isolated Au nanoparticles favorably lead to byproduct formation.

### 2.5.3. Impact of Calcium Hydroxide Content

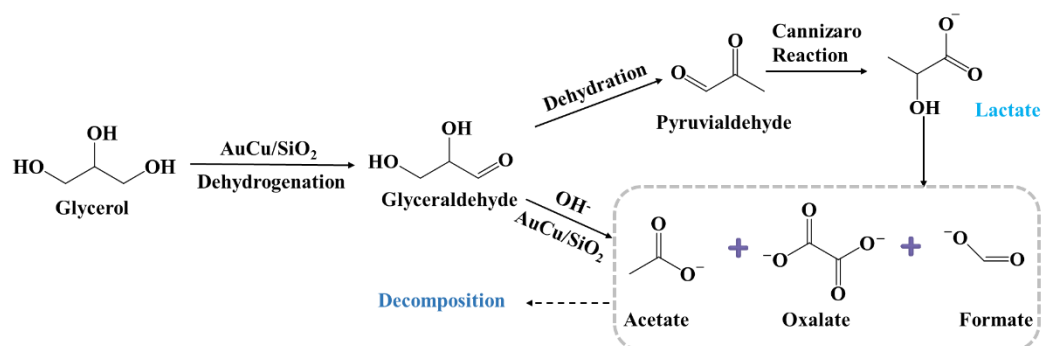When the reaction of glycerol with calcium hydroxide at various mole ratios was catalyzed by the $Au_{0.5}Cu_{10}/SiO_2$ catalyst at 200 °C for 0.5–4 h, the glycerol conversion remarkably increased, whereas the calcium lactate selectivity slightly decreased with the increase in the initial mole ratio of calcium hydroxide to glycerol and the extension of the reaction time (Figure 6a,b). When the initial mole ratios of calcium hydroxide to glycerol were 0.6:1 and 0.8:1 at the reaction time of 2 h, glycerol conversions were 94% and 96%, respectively (Figure 6a). Selectivities of calcium lactate arrived at 91% (Figure 6b). Selectivities of calcium formate, acetate, and oxalate slightly increased with the increase in the initial mole ratio of calcium hydroxide to glycerol, but slightly decreased with the extension of the reaction time (Figure 6c–e).



**Figure 6.** Reaction of glycerol with calcium hydroxide at different ratios catalyzed by the $Au_{0.5}Cu_{10}/SiO_2$ catalyst. Glycerol aqueous solution, 2 mol·L$^{-1}$; reaction temperature, 200 °C; catalyst, 9.2 g·L$^{-1}$. (**a**) Glycerol conversion and (**b**–**e**) selectivities of calcium lactate, formate, acetate, and oxalate.

Reaction routes in the catalytic reaction of glycerol with calcium hydroxide are illustrated in Scheme 1 according to the experimental results. The bimetallic $Au_{0.5}Cu_{10}/SiO_2$ catalyst catalyzed the dehydrogenation of glycerol to glyceraldehyde [10,30,31], which
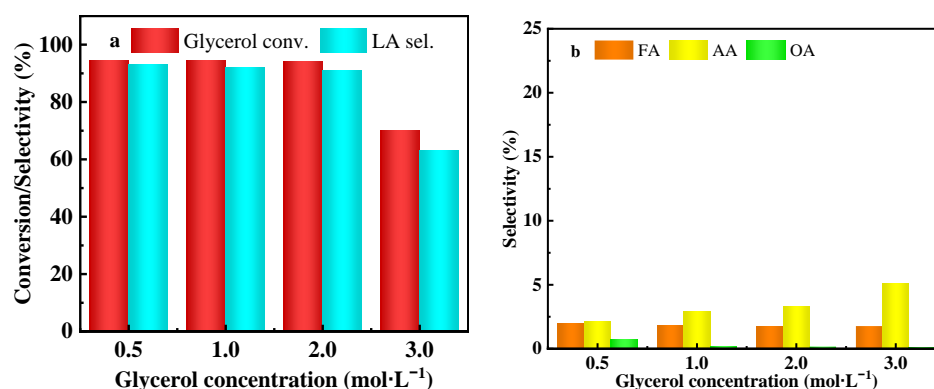
is a slower reaction process because glyceraldehyde could not be identified under our experimental conditions. Glyceraldehyde could be catalytically dehydrated to form pyruvaldehyde by $OH^-$ anions and the resultant pyruvaldehyde can be converted to calcium lactate [10,31,32]. The intermediates, glyceraldehyde and pyruvaldehyde, could also not be identified in our experiments, which indicates that the dehydration of glyceraldehyde and conversion of pyruvaldehyde are rapid reactions. The formation of oxalate, formate, and acetate could be through the decomposition of the intermediate and lactate catalyzed by $OH^-$ anions [10]. The decrease in contents of oxalate, formate, and acetate with an extended reaction time is probably caused by their decomposition in an alkaline atmosphere.



**Scheme 1.** Reaction routes in the catalytic reaction of glycerol with calcium hydroxide in an aqueous solution on bimetal $AuCu/SiO_2$ catalysts [10,30,32].

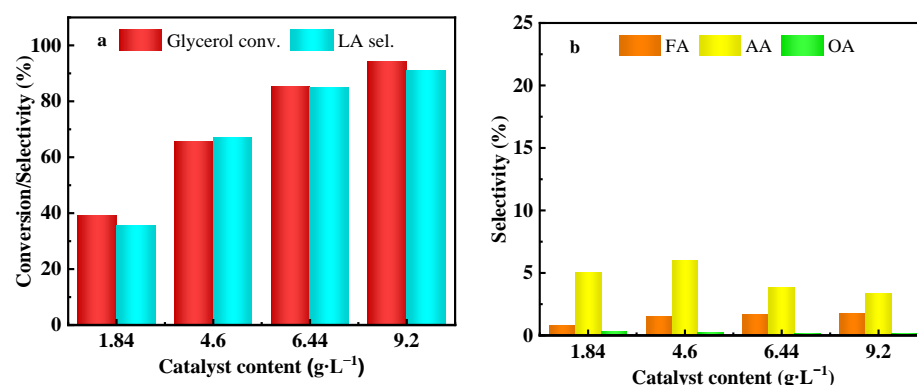### 2.5.4. Impacts of Glycerol Concentration and Catalyst Content

At initial glycerol concentrations of 0.5–2.0 mol·$L^{-1}$ and a mole ratio of calcium hydroxide to glycerol of 0.6:1, after reacting at 200 °C for 2 h on the $Au_{0.5}Cu/SiO_2$ catalyst, the glycerol conversions were above 94% at a calcium lactate selectivity of larger than 91% (Figure 7). When the glycerol concentration was further increased to 3.0 mol·$L^{-1}$, the glycerol conversion and calcium lactate selectivity remarkably declined to 70% and 63%, respectively. We suggest that the optimal concentration of glycerol is 2 mol·$L^{-1}$ for obtaining a higher calcium lactate yield under our present experimental conditions.



**Figure 7.** Reaction of glycerol with calcium hydroxide catalyzed by the $Au_{0.5}Cu_{10}/SiO_2$ catalyst. Glycerol aqueous solution, 0.5–3 mol·$L^{-1}$; initial mole ratio of calcium hydroxide to glycerol at 0.6:1; catalyst, 9.2 g·$L^{-1}$; reaction time, 2 h at 200 °C. (**a**) Glycerol conversion and calcium lactate selectivity and (**b**) selectivities of calcium acetate, formate, and oxalate.

When the reaction of glycerol (2 mol·$L^{-1}$) with calcium hydroxide at an initial mole ratio of calcium hydroxide to glycerol of 0.6:1 was catalyzed by the $Au_{0.5}Cu_{10}/SiO_2$ catalyst with catalyst contents of 1.84–9.2 g·$L^{-1}$ at 200 °C for 2 h, glycerol conversion and calcium lactate selectivity were obviously improved with the increase in catalyst content (Figure 8). With a catalyst content of 9.2 g·$L^{-1}$, the glycerol conversion reached 94% at a calcium lactate

selectivity of 92%. Obviously, a high catalyst content is profitable for the catalytic reaction of glycerol with calcium hydroxide to calcium lactate.



**Figure 8.** Reaction of glycerol with calcium hydroxide catalyzed by the $Au_{0.5}Cu_{10}/SiO_2$ catalyst. Glycerol aqueous solution, 2 mol·L$^{-1}$; initial mole ratio of calcium hydroxide to glycerol at 0.6:1; catalyst, 1.84–9.2 g·L$^{-1}$; reaction time, 2 h at 200 °C. (**a**) Glycerol conversion and calcium lactate selectivity and (**b**) selectivities of calcium acetate, formate, and oxalate.

### 2.6. Reaction Kinetics Simulation

To ascertain the impacts of the temperature, glycerol concentration, calcium hydroxide concentration, and catalyst content on the glycerol conversion rate, the reaction rate of glycerol consumption was simulated by utilizing an empirical power-function type reaction kinetics equation.

$$-r_A = -\frac{dn_A}{Vdt} = kC_A^a C_B^b C_{cat}^c \tag{1}$$

$$k = A exp(-E_a/(RT)) \tag{2}$$

where $k$ is the rate constant. $a$, $b$, and $c$ are the reaction orders for glycerol concentration ($C_A$, mol·L$^{-1}$), calcium hydroxide concentration ($C_B$, g·L$^{-1}$), and catalyst concentration ($C_{cat}$, g·L$^{-1}$), respectively.

Although it is difficult to dissolve Ca(OH)$_2$ in water, the produced lactate anion could rapidly react with Ca$^{2+}$ to form easily soluble calcium lactate. The concentration of Ca(OH)$_2$ is the whole mass concentration because the amount of Ca(OH)$_2$ significantly affects the reaction. The catalyst concentration is the whole mass concentration.

Combing Equations (1) and (2) and taking the natural logarithm on both sides of the resultant equation yields Equation (3) in linear form.

$$\ln(-r_A) = lnA - Ea/RT + alnC_A + blnC_B + clnC_{cat} \tag{3}$$

Initial conversion rates of glycerol for the first 0.5 h under various reaction conditions were used for the reaction kinetics simulation by the linear regression method (Table S1). The simulated reaction kinetics equation with a correlation coefficient of 0.97 is listed as Equation (4). The higher correlation coefficient indicates that the reaction kinetic equation is well simulated using the reaction data under various reaction conditions.

$$-r_A = -dn_A/Vdt = 247.87 \exp\left(-\frac{44,305.3}{RT}\right) C_A^{0.23} C_B^{1.04} C_{cat}^{0.7} \tag{4}$$

The simulated reaction activation energy (*Ea*) is 44.3 kJ·mol$^{-1}$, which implies that glycerol conversion can be conducted by overcoming a mild energy barrier. According to the reaction orders, the impacts of concentrations of glycerol, calcium hydroxide, and catalyst on glycerol conversion rate are in the order of Ca(OH)$_2$ > catalyst > glycerol.

Researchers reported that when the oxidation of glycerol to lactic acid was catalyzed by a CuO/C catalyst in a NaOH aqueous solution, the activation energy was

134.39 kJ·mol$^{-1}$ [26]. The reaction activation energies for glycerol conversion to lactic acid on bimetallic CuAu$_1$, CuAu$_2$, CuAu$_3$, and CuAu$_4$ catalysts were 64.0, 53.4, 46.8, and 36.9 kJ·mol$^{-1}$, respectively [33]. Furthermore, Hausoul et al. [34] reported that in the hydrogenolysis of glycerol on the Pt/C catalyst, alkaline earth metal hydroxides improved the reaction. Therefore, we suggest that bimetallic CuAu and Ca(OH)$_2$ facilitate glycerol conversion, which leads to a lower activation energy.

## 3. Experimental

### 3.1. Materials

Glycerol (99%), acetic acid (99.5%), oxalic acid (99.5%), lactic acid (85%), Cu(NO)$_3$·3H$_2$O (99%), HAuCl$_4$·4H$_2$O (Au, 47.8 wt%), hydrazine hydrate (85%), sodium hydroxide (NaOH, 96%), phosphoric acid (H$_3$PO$_4$, 85%), concentrated hydrochloric acid (HCl, 37%), disodium hydrogen phosphate (99%), *n*-butanol (99.5%), and methanol (HPLC, 99.8%) were supplied by the Dewei Chem. Reagent Co., Zhenjiang, China. Formic acid (88%) was supplied by the Nanjing Chem. Reagent Co., Nanjing, China. Silicon dioxide (average particle size, 13 nm) was supplied by the Hailong Nuclear Mater. Technol. Co., Zhenjiang, China.

### 3.2. Preparation of AuCu/SiO$_2$ Nanocatalysts

Bimetallic AuCu/SiO$_2$ nanocatalysts were prepared using the wet chemical reduction technique. First, 9.0 g of silicon dioxide was added to 40 mL of Cu(NO)$_3$·3H$_2$O (0.4 mol·L$^{-1}$) aqueous solution. After the suspension was stirred at 40 °C for 1 h, a NaOH (4 wt%) aqueous solution was added dropwise to adjust the pH to 11.5. When the above-mentioned suspension was continuously stirred for 1 h, a prescribed volume of HAuCl$_4$·4H$_2$O (1 wt%) aqueous solution was slowly dropped under stirring for 1 h and the pH value was maintained at 11.5. To reduce active components, hydrazine hydrate with a hydrazine hydrate/total metal ion molar ratio of 10:1 was added dropwise at 0.5 h. After reducing for 4 h, the resultant AuCu/SiO$_2$ catalyst samples were separated by centrifugation at a rotation rate of 10,000 rpm for 15 min and washed with pure water to eliminate sodium salts. The residual concentrations of gold and copper components in the water phase were negligibly detected by ICP measurement, which indicates that gold and copper components could be completely loaded onto SiO$_2$ support. The as-prepared AuCu/SiO$_2$ nanocatalysts were kept in anhydrous ethanol to prevent oxidation by oxygen from the atmosphere. The catalysts were denoted as Au$_m$Cu$_n$/SiO$_2$ and m and n were the mass percentages of Au and Cu components in catalysts.

### 3.3. Characterization

Crystal structures and morphologies of the as-prepared AuCu/SiO$_2$ nanocatalysts were examined on a powder X-ray diffractometer (D8 super speed Bruker-AEX Co. (Billerica, MA, USA), Cu K$\alpha$ radiation at $\lambda$ of 1.54056 Å) and a transmission electron microscope (JEM-2100, JEOL Ltd., Tokyo, Japan, 200 kV). Particle sizes of metallic Au$^0$ and Cu$^0$ nanoparticles on silicon dioxide nanoparticle supports were measured by combining both TEM and HRTEM analyses. The particle sizes were directly measured from TEM images of at least 50 individual particles.

X-ray photoelectron spectra of the AuCu/SiO$_2$ nanocatalysts were acquired on an ESCALAB 250 spectrometer (Thermo Fisher Scientific, Waltham, MA, USA). Binding energies of Au, Cu, and Si components in catalysts were calibrated by referencing the C1s peak at 284.8 eV of contaminated carbon.

To determine surface areas and pore sizes of the AuCu/SiO$_2$ nanocatalysts, their N$_2$ adsorption–desorption isotherms were acquired by utilizing a NOVA 2000e physical adsorption apparatus at −196 °C (Quantachrome, Boynton Beach, FL, USA).

### 3.4. Catalysis

The synthesis of calcium lactate was catalyzed by the as-prepared AuCu/SiO$_2$ nanocatalysts through a glycerol dehydrogenation reaction in a calcium hydroxide aqueous solution

under a nitrogen atmosphere. The prescribed quantities of glycerol, calcium hydroxide, and catalysts were added to deionized water to obtain 100 mL of reaction mixture in a 1 L steel stainless autoclave. After a pure nitrogen (99.999%) stream was introduced into the reactor to replace air inside for at least 0.25 h, reaction temperatures were raised to prescribed values by heating the autoclave with the use of a 1200 W electric oven outside. As the reaction temperatures arrived at prescribed values, stirring started at 500 rpm, and the timing of the reaction was started.

After reacting for a prescribed time, the spent $AuCu/SiO_2$ catalyst was filtrated from the reaction mixture at 80 °C. The filtrate was acidified with concentrated hydrochloric acid to a pH of around 1.0 and analyzed using the high-performance liquid chromatography(Agilent 1290 Infinity II, Agilent Technologies, Santa Clara, CA, USA), utilizing a reversed-phase C18 column (Wonda Cr act ODS-2, 5 μm, 4.6 × 250 nm) at 35 °C. $H_3PO_4/Na_2HPO_4$ (20 mmol·$L^{-1}$ $Na_2HPO_4$, acidified by $H_3PO_4$ to pH = 2.5) aqueous solution and methanol (*v:v* = 90:10) were mixed and utilized as the mobile phase with a volumetric flowing rate at 0.7 mL·$min^{-1}$. Products were identified by comparison with the retention times of standard samples, and their compositions were quantified by an external standard method. The quantity of unreacted glycerol was quantitatively analyzed by gas chromatography (Agilent Technologies 7890A, PEG-20M, Agilent Technologies, Santa Clara, CA, USA) with an FID detector using *n*-butanol as an internal standard. The calculation of product selectivity was based on the carbon number of the product molecules.

## 4. Conclusions

$SiO_2$ nanoparticle-supported bimetallic AuCu ($AuCu/SiO_2$) nanocatalysts were prepared using the wet chemical reduction technique. The metallic $Au^0$ and $Cu^0$ nanoparticles in $AuCu/SiO_2$ catalysts experienced interactions by electron transfer from metallic Au to metallic Cu nanoparticles.

From among the $Au_{0.1-1.5}Cu_{10}/SiO_2$ catalysts, the $Au_{0.5}Cu_{10}/SiO_2$ and $Au_{0.8}Cu_{10}/SiO_2$ catalysts gave high calcium lactate yields of 87% and 86% at glycerol conversion rates of 96% and 97% when the reaction of glycerol with calcium hydroxide at an initial mole ratio of calcium hydroxide to glycerol of 0.8:1 was conducted under anaerobic atmosphere at 200 °C for 2 h. The interaction between Cu and Au nanoparticles improved the synthesis of calcium lactate through the direct reaction between glycerol and $Ca(OH)_2$ under an anaerobic condition.

The consumption rate of glycerol was well simulated with the empirical power-function type reaction kinetics, which gave the reaction activation energy (*Ea*) of 44.3 kJ·$mol^{-1}$ and the reaction orders of 0.23 for glycerol concentration, 1.04 for $Ca(OH)_2$ concentration, and 0.7 for the $Au_{0.5}Cu_{10}/SiO_2$ catalyst. The simulated reaction kinetics show that the synthesis of calcium lactate through the catalytic reaction of glycerol with calcium hydroxide could be efficiently carried out by overcoming a mild energy barrier.

The present research shows that the synthesis of calcium lactate can be efficiently and directly conducted through the catalytic reaction of glycerol with calcium hydroxide on a bimetallic $AuCu/SiO_2$ nanosized catalyst under a safe anaerobic atmosphere. This new methodology could replace the conventional calcium lactate production technique through the neutralization reaction between expensive lactic acid and $Ca(OH)_2$.

**Author Contributions:** C.L.: Experimental research, Data analysis, Writing—original draft. X.C.: Experimental research, Data analysis. A.W.: Methodology, Conceptualization, Experimental research. H.Y.: Writing—review and editing, Funding acquisition, Supervision. Y.L.: Experimental research, Data analysis. Q.L.: Experimental research, Data analysis. J.G.: Experimental research, Data analysis. All authors have read and agreed to the published version of the manuscript.

**Data Availability Statement:** Data are contained within the article.

**Conflicts of Interest:** The authors declare no conflict of interest.

## References

1. Raman, A.A.A.; Tan, H.W.; Buthiyappan, A. Two-step purification of glycerol as a value added by product from the biodiesel production process. *Front. Chem.* **2019**, *7*, 774. [CrossRef] [PubMed]
2. Global Info Research, Global Glycerol Market 2023 by Manufacturers, Regions, Type and Application, Forecast to 2029. Available online: https://www.globalinforesearch.com/search/glycerol (accessed on 26 January 2024).
3. Agrawal, D.; Budakoti, M.; Kumar, V. Strategies and tools for the biotechnological valorization of glycerol to 1, 3-propanediol: Challenges, recent advancements and future outlook. *Biotechnol. Adv.* **2023**, *66*, 108177. [CrossRef] [PubMed]
4. Xu, S.; Xiao, Y.; Zhang, W.; Liao, S.; Yang, R.; Li, J.; Hu, C. Relay catalysis of copper-magnesium catalyst on efficient valorization of glycerol to glycolic acid. *Chem. Eng. J.* **2022**, *428*, 132555. [CrossRef]
5. Liu, D.; Liu, J.-C.; Cai, W.; Ma, J.; Yang, H.B.; Xiao, H.; Li, J.; Xiong, Y.; Huang, Y.; Liu, B. Selective photoelectrochemical oxidation of glycerol to high value-added dihydroxyacetone. *Nat. Commun.* **2019**, *10*, 1779. [CrossRef] [PubMed]
6. Keogh, J.; Deshmukh, G.; Manyar, H. Green synthesis of glycerol carbonate via transesterification of glycerol using mechanochemically prepared sodium aluminate catalysts. *Fuel* **2021**, *310*, 122484. [CrossRef]
7. Pemmana, H.R.; Barnwal, P.K.; Uppaluri, R.V.S.; Peela, N.R. Selective aerobic-oxidation of glycerol to lactic acid over ruthenium-vanadium bimetallic catalysts. *J. Ind. Eng. Chem.* **2023**, *124*, 224–231. [CrossRef]
8. Wang, C.; Zhang, X.; Li, J.; Qi, X.; Guo, Z.; Wei, H.; Chu, H. Gold nanoparticles on nanosheets derived from layered rare-earth hydroxides for catalytic glycerol-to-lactic acid conversion. *ACS Appl. Mater. Interfaces* **2021**, *13*, 522–530. [CrossRef]
9. Razali, N.; Abdullah, A.Z. Production of lactic acid from glycerol via chemical conversion using solid catalyst: A review. *Appl. Catal. A Gen.* **2017**, *543*, 234–246. [CrossRef]
10. Wang, A.; Xu, Q.; Yin, H.; Xiao, L.; He, Y. Synthesis of calcium lactate starting from glycerol and calcium hydroxide catalyzed by copper-based catalysts in aqueous solution. *Mater. Sci. Eng. B* **2023**, *296*, 116678. [CrossRef]
11. Redina, E.A.; Kapustin, G.I.; Tkachenko, O.P.; Greish, A.A.; Kustov, L.M. Effect of ultra-low amount of gold in oxide supported bimetallic Au–Fe and Au–Cu catalysts on liquid-phase aerobic glycerol oxidation in water. *Catal. Sci. Technol.* **2021**, *11*, 5881–5897. [CrossRef]
12. Sever, B.; Yildiz, M. Conversion of glycerol to lactic acid over Au/bentonite catalysts in alkaline solution. *React. Kinet. Mech. Catal.* **2020**, *130*, 863–874. [CrossRef]
13. Zhang, C.; Wang, T.; Liu, X.; Ding, Y. Selective oxidation of glycerol to lactic acid over activated carbon supported Pt catalyst in alkaline solution. *Chin. J. Catal.* **2016**, *37*, 502–509. [CrossRef]
14. Evans, C.D.; Douthwaite, M.; Carter, J.H.; Pattisson, S.; Kondrat, S.A.; Bethell, D.; Knight, D.W.; Taylor, S.H.; Hutchings, G.J. Enhancing the understanding of the glycerol to lactic acid reaction mechanism over AuPt/TiO$_2$ under alkaline conditions. *J. Chem. Phys.* **2020**, *152*, 134705. [CrossRef] [PubMed]
15. Qiu, K.; Shu, Y.; Zhang, J.; Gao, L.; Xiao, G. Effective and stable zeolite imidazole framework-supported copper nanoparticles (Cu/ZIF-8) for glycerol to lactic acid. *Catal. Lett.* **2022**, *152*, 172–186. [CrossRef]
16. Moreira, A.B.F.; Nogueira, D.S.; Freitas, I.C.; Souza Júnior, R.L.; Chagas, C.A.; Souza, M.M.V.M.; Manfro, R.L. Hydrothermal transformation of glycerol to lactic acid in alkaline medium using Cu catalysts obtained from hydrotalcite-like precursors. *Waste Biomass Valori.* **2023**, *14*, 2335–2347. [CrossRef]
17. Torres, S.; Palacio, R.; López, D. Support effect in Co$_3$O$_4$-based catalysts for selective partial oxidation of glycerol to lactic acid. *Appl. Catal. A Gen.* **2021**, *621*, 118199. [CrossRef]
18. Chen, L.; Ren, S.; Ye, X.P. Lactic acid production from glycerol using CaO as solid base catalyst. *Fuel Process. Technol.* **2014**, *120*, 40–47. [CrossRef]
19. Ren, S.; Ye, X.P.; Ayers, P.D. Tandem catalytic conversion of glycerol using solid catalysts followed by transesterification to produce alkyl lactate. *RSC Adv.* **2015**, *5*, 53230–53239. [CrossRef]
20. Mann, J.B.; Meek, T.L.; Knight, E.T.; Capitani, J.F.; Allen, L.C. Configuration energies of the d-block elements. *J. Am. Chem. Soc.* **2000**, *122*, 5132–5137. [CrossRef]
21. Feng, Y.; Zhang, F.; Xuan, L.; Zhu, Y. Ionic electronegativity. *J. Dalian Inst. Light Ind.* **1998**, *17*, 70–76.
22. Yao, Y.; Wu, X.; Chen, B.; Tu, Z.; Gutiérrez, O.Y.; Cui, Y.; Wang, J.; Huang, J.; Xu, Y.; Sun, H.; et al. Copper-based catalyst confined in carbon nanocages reactor for condensed esters hydrogenation: Tuning of copper species by confined SiO$_2$ and the methanol resistance. *ACS Sustain. Chem. Eng.* **2021**, *9*, 16270–16280. [CrossRef]
23. Hernández-Ramírez, E.; Wang, J.A.; Chen, L.F.; Valenzuela, M.A.; Dalai, A.K. Partial oxidation of methanol catalyzed with Au/TiO$_2$, Au/ZrO$_2$ and Au/ZrO$_2$-TiO$_2$ catalysts. *Appl. Surf. Sci.* **2017**, *399*, 77–85. [CrossRef]
24. Zhang, A.; Zhang, L.; Jing, G.; Zhang, H.; Wang, S.; Su, H.; Zeng, S. Promotion of Au$^{3+}$ reduction on catalytic performance over the Au/CuOeCeO$_2$ catalysts for preferential CO oxidation. *Int. J. Hydrogen Energy* **2018**, *43*, 10322–10333. [CrossRef]

25. Wang, A.; Zhang, M.; Yin, H.; Liu, S.; Liu, M.; Hu, T. Direct reaction between silicon and methanol over Cu-based catalysts: Investigation of active species and regeneration of CuCl catalyst. *RSC Adv.* **2018**, *8*, 19317–19325. [CrossRef] [PubMed]

26. Li, S.; Li, S.M.; Wang, Y.; Tang, C.; Qiu, L.; Yu, S. Selective oxidation of glycerol to lactic acid catalyzed by CuO/activated carbon and reaction kinetics. *ACS Omega* **2024**, *9*, 10583–10591. [CrossRef] [PubMed]

27. Zhang, J.; Zhu, G.; Wang, X.; Mai, Y.; Chen, J. Selective catalytic conversion of glycerol to lactic acid over Cu-ZnO@C catalysts. *Catal. Commun.* **2023**, *181*, 106733. [CrossRef]

28. Yin, H.X.; Zhang, C.; Yin, H.; Gao, D.; Shen, L.; Wang, A. Hydrothermal conversion of glycerol to lactic acid catalyzed by Cu/hydroxyapatite, Cu/MgO, and Cu/ZrO$_2$ and reaction kinetics. *Chem. Eng. J.* **2016**, *288*, 332–343. [CrossRef]

29. Liu, H.; Huang, Z.; Xia, C.; Jia, Y.; Chen, J.; Liu, H. Selective hydrogenolysis of xylitol to ethylene glycol and propylene glycol over silica dispersed copper catalysts prepared by a precipitation–gel method. *ChemCatChem* **2014**, *6*, 2918–2928. [CrossRef]

30. Liu, L.; Ye, X.P. Simultaneous production of lactic acid and propylene glycol from glycerol using solid catalysts without external hydrogen. *Fuel Process. Technol.* **2015**, *137*, 55–65. [CrossRef]

31. Wang, A.; Xu, Q.; Yin, H. Synthesis of lactic acid starting from glycerol catalyzed by CaO supported CuO and metallic Cu catalysts in Ca(OH)$_2$ aqueous solution. *React. Kinet. Mech. Catal.* **2022**, *135*, 3205–3221. [CrossRef]

32. Roy, D.; Subramaniam, B.; Chaudhari, R.V. Cu-based catalysts show low temperature activity for glycerol conversion to lactic acid. *ACS Catal.* **2011**, *1*, 548–551. [CrossRef]

33. Shen, L.; Zhou, X.; Wang, A.; Yin, H.; Yin, H.X.; Cui, W. Hydrothermal conversion of high-concentrated glycerol to lactic acid catalyzed by bimetallic CuAu$_x$ (x = 0.01–0.04) nanoparticles and their reaction kinetics. *RSC Adv.* **2017**, *7*, 30725–30739. [CrossRef]

34. Beine, A.K.; Wang, X.; Vennewald, M.; Schmidt, R.U.S.; Glotzbach, C.; Palkovits, R.; Hausoul, P.J.C. On the effect of alkaline earth metal cations in the hydrogenolysis of glycerol over Pt/C—An experimental and theoretical study. *ChemCatChem* **2022**, *14*, e202101940. [CrossRef]